Scientific Research Publishing

Open Journal of Fluid Dynamics, 2026, 16(2), 29-49
https://www.scirp.org/journal/ojfd
ISSN Online: 2165-3860
ISSN Print: 2165-3852

Chaotic Convection in a Rotating Porous Channel Filled with (Magnetite-Copper)/Water Hybrid Nanofluid

Zinsou Rogatien Alligbe[1,2], Amoussou Laurent Hinvi[1,2,3*], Mustapha Balewa Sanni[1,2], Alain Nicaise Comlan Adomou[1,2]

[1]Laboratoire des Procédés et de l'Innovation Technologique (LaPIT), Institut National Supérieur de Technologie Industrielle (INSTI), Université Nationale des Sciences, Technologies, Ingénierie et Mathématiques (UNSTIM), Abomey, Bénin
[2]Ecole Doctorale Sciences Technologies Ingénierie et Mathématiques (ED-STIM), Université Nationale des Sciences, Technologies, Ingénierie et Mathématiques (UNSTIM), Abomey, Bénin
[3]Laboratoire de Mécanique des Fluides, de la Dynamique Nonlinéaire et de la Modélisation des Systèmes Biologiques (LMFDNMSB), Institut de Mathématiques et de Sciences Physiques, Porto-Novo, Bénin
Email: *hinvi.laurent@unstim.bj

How to cite this paper: Alligbe, Z.R., Hinvi, A.L., Sanni, M.B. and Adomou, A.N.C. (2026) Chaotic Convection in a Rotating Porous Channel Filled with (Magnetite-Copper)/Water Hybrid Nanofluid. *Open Journal of Fluid Dynamics*, **16**, 29-49.
https://doi.org/10.4236/ojfd.2026.162003

Received: March 7, 2026
Accepted: May 15, 2026
Published: May 18, 2026

Abstract

The technological challenge lies in developing new processes that allow for more efficient heat transfer management in industrial operations. It is with this in mind that the present work focuses on the thermoconvection of a (magnetite-copper)/water saturating a rotating porous channel. To this end, we used the Darcy-Bénard convection model to model the equations of motion, the Fourier law for the heat transfer and concentration equations. The minimum-order double Fourier series method is used to transform it into a system of six nonlinear equations. The regular and chaotic motion of the nonlinear system is studied using the Runge-Kutta algorithm. The effects of various dimensionless parameters and the physicochemical properties of nanoparticles on the dynamic system are analyzed using bifurcation diagrams, Lyapunov diagrams, phase spaces and time evolution. Numerical results obtained confirm that the system can shift between regular and chaotic behavior, or vice versa, alternating with period-splitting phenomena.

Keywords

Magnetite-Copper, Nanoliquid, Double-Diffuse Convection, Bifurcation

1. Introduction

Over the past few decades, the study of thermal convection of fluids in porous media

has attracted growing interest due to the many applications in the fields of energy engineering, heat storage, cooling systems, and industrial processes [1] [2]. In fluid-saturated porous media, convective motions can develop, giving rise to a variety of dynamic behaviors ranging from simple steady states to highly complex states, including oscillations, periodicity, and chaos. The aluminatantalum nanofragments, adding a magnetic field and/or a rotational force, have the stabilising and controlling effects on the onset of thermal instability and chaotic convection in engine oil [3]. In this context, chaotic convection becomes a priority in scientific research because it is associated with enhanced heat transfer, dynamical effects sensitive to initial conditions, and coexistence of attractors. The initial work on simple or hybrid nanofluids and on chaotic convection in porous media was based respectively on the importance of this new category of fluids in dynamic systems and on reduced Lorenz-type models to describe the transition between stationary convection and complex regimes, particularly for low Prandtl numbers. The concept of nanofluids, introduced by Choi and Eastman [4], is based on the dispersion of solid nanoparticles of nanometric size in a base fluid such as water, oil, or ethylene glycol, in order to improve thermal conductivity and, consequently, heat transfer performance. Since then, nanofluids have been the subject of numerous theoretical, numerical, and experimental investigations [5] [6]. The convection of nanofluids has been widely studied in several geometric configurations. These studies have shown that nanoparticles affect thermal stability, flow structures, and average Nusselt number [7] [8]. Furthermore, the introduction of an external magnetic field has opened the way for magnetohydrodynamic (MHD) analysis of nanofluids, revealing that the magnetic field can dampen or control the convective flow depending on the field strength and the electrical properties of the fluid [8] [9].

However, it appears that simple nanofluids with a single species of nanoparticles have limitations, such as unsatisfactory thermal enhancement, long-term stability issues, and limited flow control. To correct this phenomenon, the concept of hybrid nanofluid, based on the combination of two or more types of nanoparticles, has been introduced. This approach allows taking into account the combined effects of the different nanoparticles to simultaneously improve the thermal, dynamic, and electromagnetic properties of the fluid [5] [10]. In this framework, we have chosen the hybrid nanofluids (Fe_3O_4-Cu)/water for our study. Copper (Cu), known for its very high electrical and thermal conductivity, combined with magnetite Fe_3O_4 for its remarkable magnetic properties, gives the hybrid fluid (Fe_3O_4-Cu)/water thermophysical and dynamic characteristics superior to those of simple nanofluids. Several studies have shown that the introduction of Fe_3O_4 allows more effective control of flow under a magnetic field, while the presence of Cu significantly improves overall heat transfer [11] [12]. Abedini *et al.* [10] in particular analyzed the MHD flow and heat transfer of a (Cu-Fe_3O_4)/water hybrid nanofluid near a moving surface, highlighting superior performance to conventional nanofluids. The influence of control parameters such as the Rayleigh number, the Hartmann number, the Prandtl number, and the volume fraction of na-

noparticles on the convection of the particules/water or oil hybrid nanofluid has been highlighted in several recent studies [3] [10] [13] [14]. It has been shown that increasing the Hartmann number generally tends to stabilize the flow by attenuating the convective motions, while high Rayleigh number values favor the intensification of convection and heat transfer. These coupled effects attest to the influence of the magnetic character of iron oxide (Fe_3O_4) on the dynamics of the hybrid fluid. But the effect of the Solutal Rayleigh number has been little studied in the literature. Beyond steady state regimes, the study of unsteady and chaotic convection in hybrid nanofluids is very important due to their high-performance industrial applications. Previous work on thermosoluble and double diffusive convection has shown that convective systems sometimes undergo complex transitions from steady regimes to periodic, then chaotic regimes, via successive bifurcations [15] [16]. These transitions are manifested by the appearance of bifurcations, period doublings, and positive Lyapunov exponents, characteristics of chaos. Furthermore, in order to better describe the propagation of heat in complex fluids, non-classical models of thermal conduction have been proposed. The Maxwell-Cattaneo model, developed to remedy the paradox of the instantaneous propagation of heat induced by Fourier's law, introduces a thermal relaxation time in the heat flux equation [17] [18]. The integration of this model in the study of the thermal convection of nanofluids and hybrid nanofluids has shown that thermal relaxation can delay the appearance of convective instability and modify the nature of the bifurcations leading to chaos. Motivated by all these works, the present paper aims to analyze the chaotic double-diffuse Darcy-Bénard convection [19] in a hybrid nanofluid (Fe_3O_4-Cu)/water saturating a rotating porous medium. The study will combine theoretical and numerical approaches in order to better understand the complex thermal dynamics of the system, incorporating double thermal diffusion. Specifically, it will involve mathematically formalizing the model; determining the fixed points of the resulting modified Lorenz system; studying the effects of nanoparticle volume fractions on the convection of the hybrid nanofluid and analyzing the influence of Thermal Rayleigh, Solutal Rayleigh, Darcy and Taylor numbers on the convection. To achieve this, we used the double Fourier series to find the modified Lorenz system corresponding to our model. We used the fourth-order Runge-Kutta method in Fortran to simulate and construct bifurcation diagrams for different values of the parameters characterizing the system. To confirm the dynamics highlighted by the bifurcation diagrams, we plotted the associated Lyapunov exponent for each case and then plotted some phase spaces and time evolutions. To this end, in the following section, we will model the flow of the (magnetite-copper)/water hybrid nanofluid using partial differential equations of mass, momentum, energy and concentration conservation, which will be transformed into ordinary differential equations using the truncated Galerkin method. In the third section, the resulting system of nonlinear equations will be analyzed according to the theory of dynamical systems. The fourth section will be dedicated to the results and their discussion, and the conclusion to the fifth and final section.

2. Mathematical Modeling

Consider a porous medium saturated with a (Cu-Fe_3O_4)/water hybrid nanofluid, incompressible and rotating at a constant speed $\boldsymbol{\Omega}$ around a vertical axis. This medium, within which there is uniform gravity $\vec{g}$ field, is bounded by two infinitely long horizontal plates subjected to a vertical temperature and concentration gradient through the hybrid nanofluid. The upper plate is at temperature $T_H = T_c$ and concentration $S_H = S_C$, while the lower plate is at temperature $T_l = T_C + \Delta T$ and concentration $S_l = S_C + \Delta S$. An orthonormal Cartesian coordinate system is adopted with unit vectors $\boldsymbol{e}_x$, $\boldsymbol{e}_y$ and $\boldsymbol{e}_z$ where the origin coincides with the lower boundary of the channel and the z-axis is vertical. The thermal, mechanical and solubility properties in the x and y directions are assumed to be identical. The flow obeys Darcy-Bénard convection's law and, taking into account the Boussinesq approximations, the density can be described by

$$\rho = \rho_{hnf}\left[1-\beta_{hnf}\left(T-T_c\right)+\beta_S\left(S-S_c\right)\right], \tag{1}$$

where β_{hnf} and β_S are volume dilatation coefficients due to variations in temperature, nanoparticles concentration, ρ_{hnf} is the density of the hybrid nanofluid and S is the concentration of solution.

The geometry of this considered problem is presented in Figure 1.

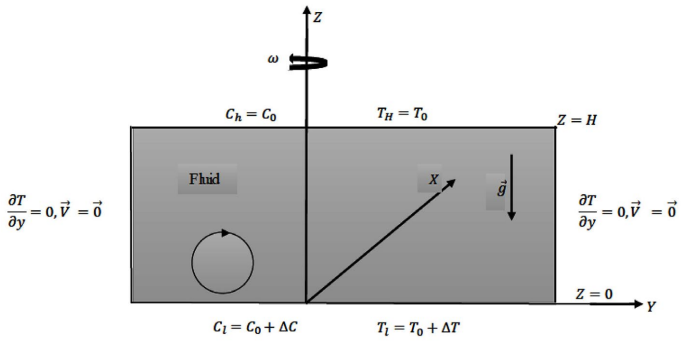

Figure 1. Physical model of our problem.

The upper and lower walls are subject to the following temperature and solute concentration conditions:

$T_l = T_c + \Delta T$ at $z = 0$ and $T_H = T_C$ at $z = H$,

$S_l = S_c + \Delta S$ at $z = 0$ and $S_H = S_C$ at $z = H$.

Therefore, fluid flow in the horizontal, infinite porous cavity supported by double diffusion convection is governed by the set of equations governing the conservation of mass, momentum, energy, and concentration, given by:

$$\begin{cases} \nabla \cdot \boldsymbol{V} = 0, \\ \dfrac{\rho_{hnf}}{\varepsilon}\left(\dfrac{\partial \boldsymbol{V}}{\partial t}+\left(\boldsymbol{V}\cdot\nabla\right)\dfrac{\boldsymbol{V}}{\varepsilon}\right) = -\nabla p + \dfrac{\mu_{hnf}}{\varepsilon}\nabla^2\boldsymbol{V} + \rho\boldsymbol{g} - \dfrac{\mu_{hnf}}{K}\boldsymbol{V} - \dfrac{2\rho_{hnf}}{\varepsilon}\left(\boldsymbol{\Omega}\wedge\boldsymbol{V}\right), \\ \left(\rho C_p\right)_{hnf}\dfrac{\partial T}{\partial t}+\left(\rho C_p\right)_{hnf}\left(\boldsymbol{V}\cdot\nabla\right)T = k_{hnf}\nabla^2 T, \\ \left(\rho C_p\right)_s\dfrac{\partial S}{\partial t}+\left(\rho C_p\right)_s\left(\boldsymbol{V}\cdot\nabla\right)S = k_S\nabla^2 S, \end{cases} \tag{2}$$

where: μ_{hnf}, $\left(\rho C_p\right)_{hnf}$, k_{hnf}, $\left(\rho C_p\right)_s$, ε, k_s are respectively dynamic viscosity of the hybrid nanofluid, heat capacity of the hybrid nanofluid, thermal conductivity of the hybrid nanofluid, heat capacity of the nanoparticle, porosity of the cavity, nanoparticle diffusivity; $\boldsymbol{V}=(u,v,w)$ is the velocity component. The subscripts: $*,c,f,hnf,s,0$ are respectively for dimensionless critical, base fluid, hybrid nanofluid, nanoparticles and reference state; $\boldsymbol{\nabla}=\frac{\partial}{\partial x}\boldsymbol{e}_x+\frac{\partial}{\partial y}\boldsymbol{e}_y+\frac{\partial}{\partial z}\boldsymbol{e}_z$ is the gradient vector and $\boldsymbol{\nabla}^2=\frac{\partial^2}{\partial x^2}+\frac{\partial^2}{\partial y^2}+\frac{\partial^2}{\partial z^2}$.

The velocity component along the x-axis is zero. Thus, the equations governing the hybrid nanofluid flow are reduced to 2-D, then there exists a current function $\varphi(t,y,z)$ such that $\boldsymbol{V}=v\boldsymbol{e}_y+w\boldsymbol{e}_z=\frac{\partial\varphi}{\partial z}\boldsymbol{e}_y-\frac{\partial\varphi}{\partial y}\boldsymbol{e}_z$. The boundary conditions are described as follows:

$$\left.\begin{array}{ll} T=T_l=T_C+\Delta T & \text{at } z=0,\\ T=T_H=T_C & \text{at } z=H,\\ S=S_l=S_C+\Delta S & \text{at } z=0,\\ S=S_H=S_C & \text{at } z=H,\\ \boldsymbol{V}=\boldsymbol{0} & \text{at } z=0,H. \end{array}\right\} \tag{3}$$

By non-dimensionalizing the transport, concentration and heat transfer equations using the following quantities:

$$y=Hy_*,\quad Z=hz_*,\quad t=\frac{t_*H^2}{\alpha_f},\quad v=\frac{\alpha_f}{Hv_*},$$

$$w=\frac{\alpha_f}{Hw_*},\quad p=\frac{\rho_f\alpha_f^2p_*}{H},\quad T_*=\frac{T-T_C}{\Delta T_C},\quad S_*=\frac{S-S_C}{\Delta S_C},$$

where $\boldsymbol{V}_*=(0,v_*,w_*)$ is the velocity component, p_* is the pressure, (T_*-T_C) and (S_*-S_C) are the temperature and solute concentration variations, α_f is the thermal diffusivity of the base fluid, and by replacing the variables defined above in the system Equations (2), we obtained after omitting (*) and neglecting the vorticity term $(\boldsymbol{V}\cdot\boldsymbol{\nabla})\boldsymbol{V}$ and the viscous force term $\boldsymbol{\nabla}^2\boldsymbol{V}$ according to Darcy-Bénard convection [19], the following dimensionless equations:

$$\begin{cases} \boldsymbol{\nabla}\cdot\boldsymbol{V}=0,\\ \left(\frac{\gamma_1}{V_a}\frac{\partial}{\partial t}+1\right)\boldsymbol{V}=-\frac{\gamma_1D_a}{P_r}\boldsymbol{\nabla}P-\frac{\gamma_1D_aT_a}{\varepsilon}(\boldsymbol{e}_z\wedge\boldsymbol{V})-\gamma_1D_aR_0\boldsymbol{e}_z\\ \qquad\qquad +M_2D_aR_aT\boldsymbol{e}_z-\gamma_1D_aR_sS\boldsymbol{e}_z,\\ \frac{\partial T}{\partial t}+\boldsymbol{V}\cdot\boldsymbol{\nabla}T=\gamma_4\boldsymbol{\nabla}^2T,\\ \frac{\partial S}{\partial t}+\boldsymbol{V}\cdot\boldsymbol{\nabla}S=\gamma_5\boldsymbol{\nabla}^2S, \end{cases} \tag{4}$$

where: $P_r=\frac{\nu_f}{\alpha_f}$, $V_a=\frac{\varepsilon P_r}{D_a}$, $R_a=\frac{\beta_f\Delta T_cgH^3}{\alpha_f\nu_f}$, $R_s=\frac{\beta_S\Delta S_cgH^3}{\alpha_f\nu_f}$, $D_a=\frac{K}{H^2}$,

$T_a = \dfrac{2\Omega K}{\nu_f D_a}$ are respectively: Prandtl, Vadasz, Thermal Rayleigh, Solutal Rayleigh, Darcy and Taylor numbers. The parameter γ_i, M_i and other parameters are expressed as:

$$\gamma_1 = \left(\frac{\rho_{hnf}}{\rho_f}\right)\left(\frac{\mu_f}{\mu_{hnf}}\right), \gamma_2 = \left(\frac{\sigma_{hnf}}{\sigma_f}\right)\left(\frac{\rho_f}{\rho_{hnf}}\right), \gamma_3 = \left(\frac{\rho_f}{\rho_{hnf}}\right)\left(\frac{(\rho\beta)_{hnf}}{(\rho\beta)_f}\right),$$

$$\gamma_4 = \left(\frac{k_{hnf}}{k_f}\right)\left(\frac{(\rho C_p)_f}{(\rho C_p)_{hnf}}\right), \gamma_5 = \left(\frac{k_s}{k_f}\right)\left(\frac{(\rho C_p)_f}{(\rho C_p)_s}\right),$$

$$M_1 = \left(\frac{\sigma_{hnf}}{\sigma_f}\right)\left(\frac{\mu_f}{\mu_{hnf}}\right), M_2 = \left(\frac{\mu_f}{\mu_{hnf}}\right)\left(\frac{(\rho\beta)_{hnf}}{(\rho\beta)_f}\right),$$

$$R_0 = \frac{gH^3}{\nu_f \alpha_f}, \alpha_f = \frac{k_f}{(\rho C_p)_f}, \alpha_s = \frac{k_s}{(\rho C_p)_s}, \alpha_{hnf} = \frac{k_{hnf}}{(\rho C_p)_{hnf}}.$$

With the boundary conditions

$$\left.\begin{array}{ll} T = 1,\ S = 1 & \text{at } Z = 0, \\ T = 0,\ S = 0 & \text{at } Z = 1, \\ \boldsymbol{V} = \boldsymbol{0} & \text{at } Z = 0,1. \end{array}\right\} \tag{5}$$

The heat is transported only by conduction in the basic state, and the physical quantities depend only of variable z, as follows:

$$\left.\begin{array}{l} V_b = W_b = 0, \\ T_b = T_b(z) = 1 - z, \\ S_b = S_b(z) = 1 - z. \end{array}\right\} \tag{6}$$

The density, the thermal expansion coefficient, the heat capacitance, the dynamic viscosity and the thermal conductivity of the hybrid nanofluid are defined respectively as [3] [20] [21] by:

$$\rho_{hnf} = (1-\phi_2)\left((1-\phi_1)\rho_f + \phi_1 S_1\right) + \phi_2 S_2$$

$$(\rho\beta)_{hnf} = (1-\phi_2)\left((1-\phi_1)(\rho\beta)_f + \phi_1(\rho\beta)_{s_1}\right) + \phi_2(\rho\beta)_{s_2},$$

$$(\rho C_p)_{hnf} = (1-\phi_2)\left((1-\phi_1)(\rho C_p)_f + \phi_1(\rho C_p)_{s_1}\right) + \phi_2(\rho C_p)_{s_2},$$

$$\mu_{hnf} = \mu_f (1-\phi_1)^{-2.5}(1-\phi_2)^{-2.5},$$

$$k_{hnf} = k_f \left[\frac{\left(\dfrac{(\phi_1 k_{s_1} + \phi_2 k_{s_2})}{\phi} + 2k_f + 2(\phi_1 k_{s_1} + \phi_2 k_{s_2}) - 2k\phi k_{s_2}\right)}{\left(\dfrac{(\phi_1 k_{s_1} + \phi_2 k_{s_2})}{\phi} + 2k_f - 2(\phi_1 k_{s_1} + \phi_2 k_{s_2}) - 2k\phi k_{s_2}\right)}\right],$$

where ϕ_1 and ϕ_2 are respectively the volume fractions of the magnetite and copper in the hybrid nanoliquid, S_1 and S_2 their solution. The constants k_{hnf} and k_f are the thermal conductivity of the hybrid nanofluid and the base fluid, while k_{s_1} and k_{s_2} are the thermal conductivity of nanoparticle solutions.

3. Nonlinear Stability Analysis

3.1. Lorenz Modified System

To find the Lorenz modified system corresponding to our problem, after eliminating the pressure in momentum equation of system (4) (By applying the curl), we use the following double Fourier series representation (7) - (9) into the system (4)

$$\varphi(t,y,z) = A_{11}\sin ky \sin \pi z, \tag{7}$$

$$T(t,y,z) = T_b(z) + B_{11}\cos ky \sin \pi z + B_{02}\sin 2\pi z, \tag{8}$$

$$S(t,y,z) = S_b(z) + C_{11}\cos ky \sin \pi z + C_{02}\sin 2\pi z, \tag{9}$$

where $T_b(z)$ and $S_b(z)$ are defined in the system (6).

After a few operations, we find the following system of equations:

$$\begin{cases} \dfrac{\partial^2 A_{11}}{\partial \tau^2} = -\Lambda_0 \dfrac{\partial A_{11}}{\partial \tau} + \chi A_{11} + \Lambda_1 B_{11} - \Lambda_2 C_{11} + \left(\dfrac{k^2 \pi V_a D_a M_2 R_a}{a^6 \gamma_1}\right) A_{11} B_{02} \\ \qquad + \left(\dfrac{k^2 \pi V_a D_a R_S}{a^6}\right) A_{11} C_{02}, \\ \dfrac{\partial B_{11}}{\partial \tau} = -\gamma_4 B_{11} + \dfrac{k\pi}{a^2} A_{11} B_{02} + \dfrac{k}{a^2} A_{11}, \\ \dfrac{\partial B_{02}}{\partial \tau} = \dfrac{\pi}{2a^2} k A_{11} B_{11} - \dfrac{4\pi^2}{a^2} \gamma_4 B_{02}, \\ \dfrac{\partial C_{11}}{\partial \tau} = -\gamma_5 C_{11} + \dfrac{k\pi}{a^2} A_{11} C_{02} + \dfrac{k}{a^2} A_{11}, \\ \dfrac{\partial C_{02}}{\partial \tau} = -\dfrac{\pi}{2a^2} k A_{11} C_{11} - \dfrac{4\pi^2}{a^2} \gamma_5 C_{02}. \end{cases}$$

With $a^2 = k^2 + \pi^2$,

$$\Lambda_0 = 2\left(\frac{V_a}{a^2 \gamma_1}\right),$$

$$\Lambda_1 = \frac{k^2 V_a D_a M_2 R_a}{a^4 \gamma_1}\left(\frac{V_a}{a^2 \gamma_1}\right)(1-\gamma_4),$$

$$\Lambda_2 = \frac{k^2 V_a D_a M_2 R_S}{a^4 \gamma_1}\left(\frac{V_a}{a^2 \gamma_1}\right)(1-\gamma_5),$$

$$\chi = \left[-\left(\frac{2V_a}{\gamma_1}\right)\Lambda - \left(\frac{\pi T_a}{a^6}\right)\left(\frac{V_a D_a}{\epsilon}\right)^2 + \frac{k^2 V_a D_a}{a^6}\left(\frac{M_2 R_a}{\gamma_1} - R_s\right)\right].$$

Make the successful variable changes below:

$$\tau = a^2 t,\ B_{11} = \frac{\overline{B}_{11}}{R k_{cr}} = \frac{\sqrt{2}\overline{B}_{11}}{\pi R},\ A_{11} = a^2\sqrt{2}\overline{A}_{11}/k\pi,\ B_{02} = -\overline{B}_{02}/\pi R,$$

$$C_{11} = \overline{C}_{11}/R_s k_{cr} = \sqrt{2}\overline{C}_{11}/\pi R_S^*,\ C_{02} = \overline{C}_{02}/\pi R_S^*,\ R_{ac} = R_{sC} = a^6/k^2,$$

$$k_{cr} = \pi/\sqrt{2},\ \lambda = \frac{8}{\left[(k/k_{cr})^2 + 2\right]} = 4\pi^2/a^2,\ R = k^2 R_a/a^6,\ R_s^* = k^2 R_s/a^6,$$

and $\overline{A}_{11} = X\sqrt{\lambda(R-1)}$, $\overline{B}_{11} = Y\sqrt{\lambda(R-1)}$, $\overline{B}_{02} = (R-1)Z$, $\overline{C}_{11} = U\sqrt{\lambda(R-1)}$, $\overline{C}_{02} = (R-1)W$.

And by noting $\frac{\mathrm{d}\theta}{\mathrm{d}t}=\dot{\theta}$, we find the following expression:

$$\begin{cases}\dot{X}=Q,\\ \dot{Y}=-\gamma_4 Y+RX-(R-1)XZ,\\ \dot{Z}=\lambda(-\gamma_4 Z+XY),\\ \dot{U}=-\gamma_5 U+R_s^* X-(R-1)XW\\ \dot{W}=\lambda(-\gamma_5 W+XU)\\ \dot{Q}=-\delta_1 Q+\delta_2 X-\delta_3(R-)XZ+\delta_4(R-1)XW+\delta_5 Y-\delta_6 U,\end{cases}$$

with:

$$\delta_1=\frac{2V_a^*}{\gamma_1},$$

$$\delta_2=\frac{V_a^*}{\gamma_1}-T_a^* P_r^2+\frac{\varepsilon P_r R M_2}{\gamma_1}-\varepsilon P_r R_S^*,$$

$$\delta_3=\frac{\varepsilon P_r M_2}{\gamma_1},\quad \delta_4=\varepsilon P_r,\quad \delta_5=\frac{\varepsilon P_r M_2}{\gamma_1}\left(\frac{V_a^*}{\gamma_1}-\gamma_4\right),$$

$$\delta_6=\varepsilon P_r\left(\frac{V_a^*}{\gamma_1}-\gamma_5\right),\quad V_a^*=V_a/a^2,\quad T_a^*=\pi^2/a^6 T_a.$$

The system (10) is our Lorenz modified system, which models (magnetite-copper)/water hybrid nanoliquid. To test our model, we compared it to models available in the literature. So, in the absence of the rotational force and the viscous force $\gamma_5=1/L_e$ and $\gamma_1=\gamma_4=M_1=M_2=1$, $\phi_1=\phi_2=0$), our system (10) is equivalent to Idris's model [22].

Similarly, in the absence of the rotational force and the viscous force, our system (10) reduces to that of Dèdèwanou *et al.* [3] without a magnetic field. When the porosity is considered equal to 1 and the rotation and solute concentration parameters are considered zero and $\phi_1=\phi_2=0$ (ordinary fluid, water), the classical Lorenz model is recovered [13].

3.2. Dissipation and Fixed Points

The system of Equation (10) is dissipative since its trace is negative.

$$\nabla\cdot\mathcal{V}=\frac{\partial\dot{X}}{\partial X}+\frac{\partial\dot{Y}}{\partial Y}+\frac{\partial\dot{Z}}{\partial Z}+\frac{\partial\dot{U}}{\partial U}+\frac{\partial\dot{W}}{\partial W}+\frac{\partial\dot{Q}}{\partial Q}=-(\gamma_4+\lambda\gamma_4+\gamma_5+\lambda\gamma_5+\delta_1)\qquad(10)$$

Equation (10) is negative because $\gamma_4,\lambda,\gamma_5$ and δ_1 are non-zero positive constants. The system of equations is therefore dissipative. Thus, if the set of initial points in phase portrait occupies the region $\mathcal{V}(0)$ at $\tau=0$, then, after a certain time τ, the endpoints of the corresponding trajectories will fill a volume $\mathcal{V}(\tau)$ such that:

$$\mathcal{V}(\tau)=\mathcal{V}(0)\exp\left[-(\gamma_4+\lambda\gamma_4+\gamma_5+\lambda\gamma_5+\delta_1)\right].\qquad(11)$$

The expression (11) indicates that the volume decreases monotonically with time. The fixed points of the system (10) can be obtained by setting the derivatives

to zero.

$$\begin{cases} 0 = Q, \\ 0 = -\gamma_1 Y + RX - (R-1)XZ, \\ 0 = \lambda(-\gamma_4 Z + XY), \\ 0 = -\gamma_5 U + R_s^* X - (R-1)XW \\ 0 = \lambda(-\gamma_5 W + XU) \\ 0 = -\delta_1 Q + \delta_2 X - \delta_3 (R-1)XZ + \delta_4 (R-1)XW + \delta_5 Y - \delta_6 U. \end{cases}$$

The system (10) has one trivial solution that corresponds to motionless solution, that is, the origin

$$(X_0, Y_0, Z_0, U_0, W_0, Q_0).$$

With the assumption $X = Y$, we obtain two other non-trivial fixed points given by:

$$X_{1,2} = Y_{1,2} = \pm i\left(\frac{\gamma_4(\gamma_4 - R)}{R-1}\right)^{1/2}; \; Z_{1.2} = \left(\frac{\gamma_4 - R}{R-1}\right)$$

$$U_{1,2} = \pm iR_s \frac{\gamma_5\left(\frac{\gamma_4(\gamma_4 - R)}{R-1}\right)^{1/2}}{\left[\gamma_5^2 - \gamma_4(\gamma_4 - R)\right]}; \; W_{1,2} = R_s \frac{\left(\frac{\gamma_4(\gamma_4 - R)}{R-1}\right)^{1/2}}{\left[\gamma_5^2 - \gamma_4(\gamma_4 - R)\right]}; \; Q_{1,2} = 0.$$

4. Results and Discussion

In order to examine and study the chaotic convection and the various transitions in our nanoliquid hybrid (magnetite-copper)/water, numerical simulations were performed using the fourth-order Runge-Kutta method to numerically solve the nonlinear system (10). We searched for and obtained three fixed points for the system: a trivial fixed point linked to the origin, corresponding to the conducting state of the system, and two other complex conjugate fixed points corresponding to convection states. Due to the size (6 × 6) of the matrix associated with our modified Lorenz system, we were unable to analytically determine the explicit expression for the Hopf-Rayleigh bifurcation. We therefore moved on to numerical simulation using the values of thermophysical properties in Table 1 below.

Table 1. Thermophysical properties of nanofragments and base liquid [23].

	$\rho(\mathrm{kg/m^3})$	$k(\mathrm{W/m\cdot K})$	$C_p(\mathrm{J/kg\cdot K})$	$\beta(\mathrm{K^{-1}})$	$\sigma(\mathrm{S/m})$
Watter	9971	0.613	4179	21	5×10^{-2}
Magnetite	5180	9.7	670	1.3	2.5×10^{4}
Copper	8933	401	385	1.37	5.901×10^{7}

Thus, the system 10) is solved using these fourth-order Runge-Kutta algorithms in Fortran language, and the bifurcation diagrams, Lyapunov exponent, phase portraits, and time histories are plotted. According to the work of Elsaid *et al.* in [24], the chaos and regularity of a system (10) can be determined by the Lyapunov ex-

ponent defined by:

$$Lya = \lim_{\tau\to\infty} \frac{\ln\sqrt{(d\mathcal{X})^2 + (d\mathcal{Y})^2 + (d\mathcal{Z})^2 + (d\mathcal{U})^2 + (d\mathcal{W})^2 + (d\mathcal{Q})^2}}{\tau} \quad (12)$$

with $d\mathcal{X}$, $d\mathcal{Y}$, $d\mathcal{Z}$, $d\mathcal{U}$, $d\mathcal{W}$ and $d\mathcal{Q}$ are the variation of $\mathcal{X}$, $\mathcal{Y}$, $\mathcal{Z}$, $\mathcal{U}$, $\mathcal{W}$ and $\mathcal{Q}$ respectively. The system is chaotic when the largest Lyapunov exponent is positive, periodic when it is negative and quasi-periodic when it is zero.

Table 2 gives the reference values of the dimensionless parameters used for our simulations, except for cases where the effects are sought in a figure.

Table 2. Value of the reference parameter used.

Parameter	P_r	L_e	V_a	T_a	λ	D_a	ε
Value	10	0.1	100	0.1	2	0.001	0.88

We plotted bifurcation diagrams. To confirm the dynamics presented by the bifurcation diagrams, we plotted the associated Lyapunov exponent each time. To further verify the results obtained from the previous diagrams, we performed a check using phase spaces and the evolution of the amplitude as a function of time.

Figures 2-5 show the Bifurcation diagram and the corresponding Lyapunov exponent for respectively ($\phi_1 = \phi_2 = 0$) (pure water), ($\phi_1 = \phi_2 = 0.01$), ($\phi_1 = \phi_2 = 0.02$), and ($\phi_1 = \phi_2 = 0.03$) (the hybrids nanoliquid) for the other parameter values in Table 1 and Table 2.

From the four bifurcation diagrams in Figures 2-5, we observe that from the base fluid ($\phi_1 = \phi_2 = 0$)) to the hybrid nanofluids ($\phi_1 = \phi_2 \neq 0$) in the vicinity of $R = 75$, specifically $R \in]70,80[$, the chaotic dynamics gradually disappear as the volume fraction increases, giving way to regular behaviors: oscillations of period one (1) followed by period two (2), *i.e.*, period doubling for $R \in]0,123[$. This disappearance of chaotic behavior is noted from $\phi_1 = \phi_2 = 0.02$ at the level of Figure 6, where the bifurcation diagrams display regular behaviors for all $R \in]0,123[$. For the same Figures 2-5, we note chaotic behaviors for $R \in]123,160[\cup]165,200[$ and a window of regular dynamics for $R \in]160,165[$.

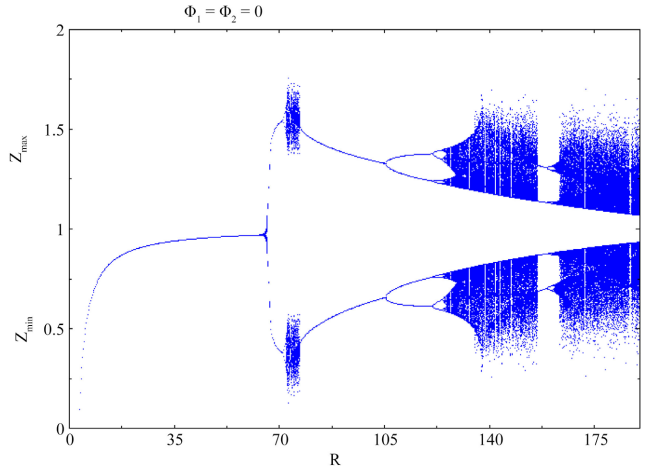

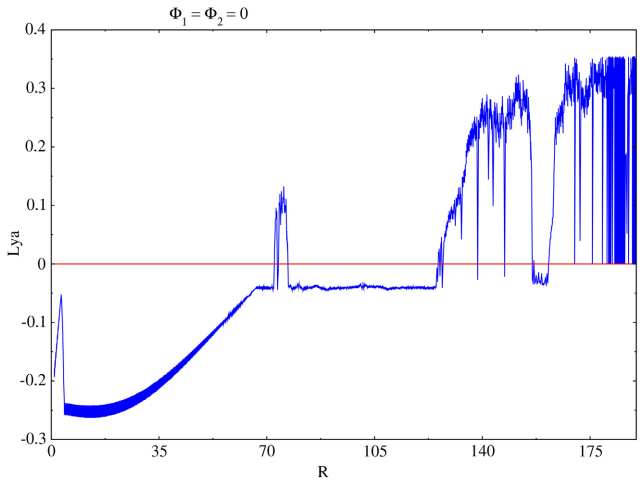

Figure 2. Bifurcation diagram and its corresponding Lyapunov exponent for pure water ($\phi_1 = 0$, $\phi_2 = 0$), with the parameter values in **Table 1** and **Table 2**.

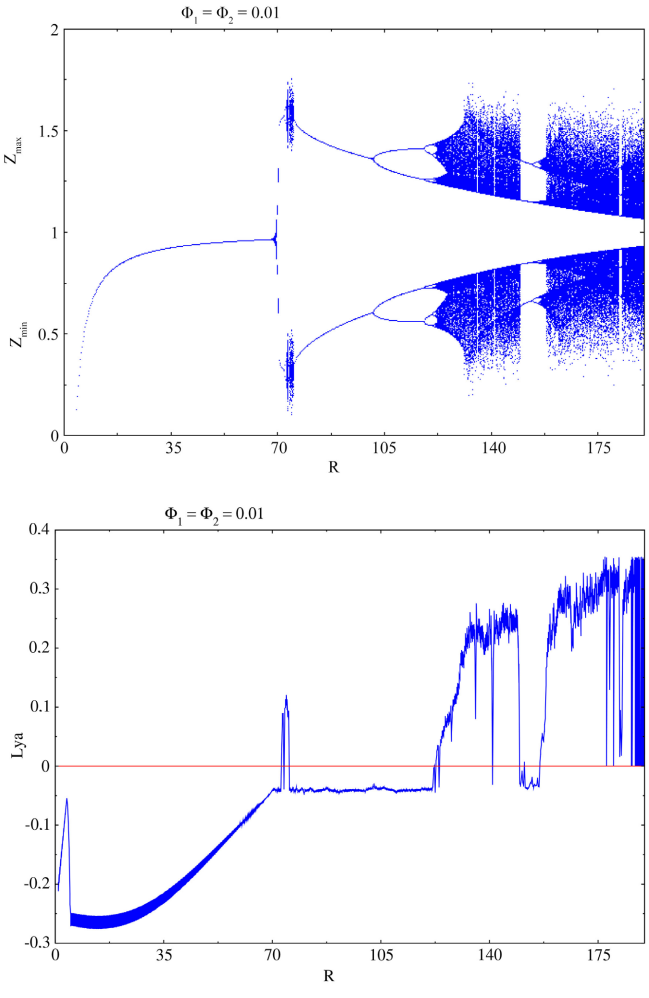

Figure 3. Bifurcation diagram and its corresponding Lyapunov exponent for (magnetite-copper)/water hybrid nanofluid ($\phi_1 = 0.01$, $\phi_2 = 0.01$) with the parameter values in **Table 1** and **Table 2**.

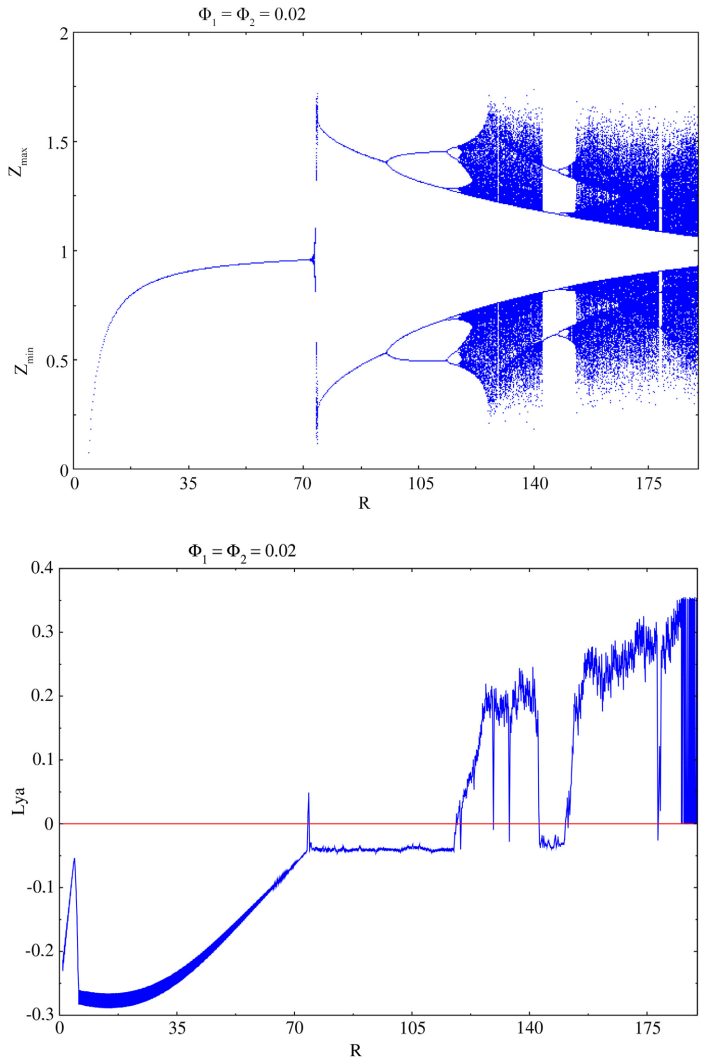

Figure 4. Bifurcation diagram and its corresponding Lyapunov exponent for (magnetite-copper)/water hybrid nanofluid ($\phi_1 = 0.02$, $\phi_2 = 0.02$), with the parameter values in **Table 1** and **Table 2**.

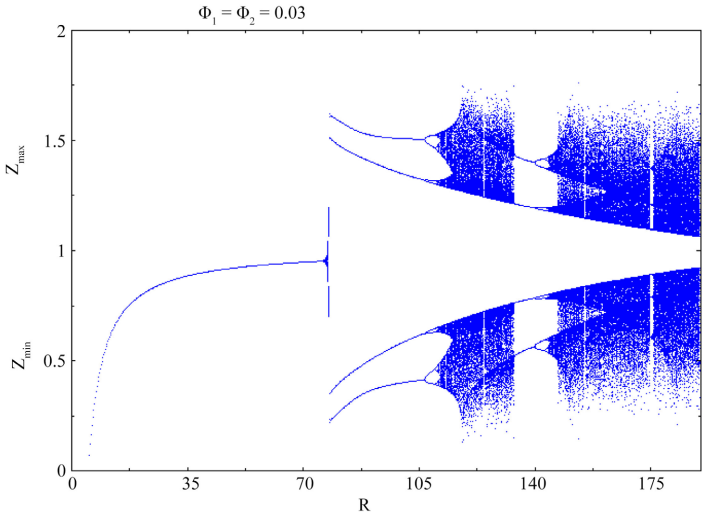

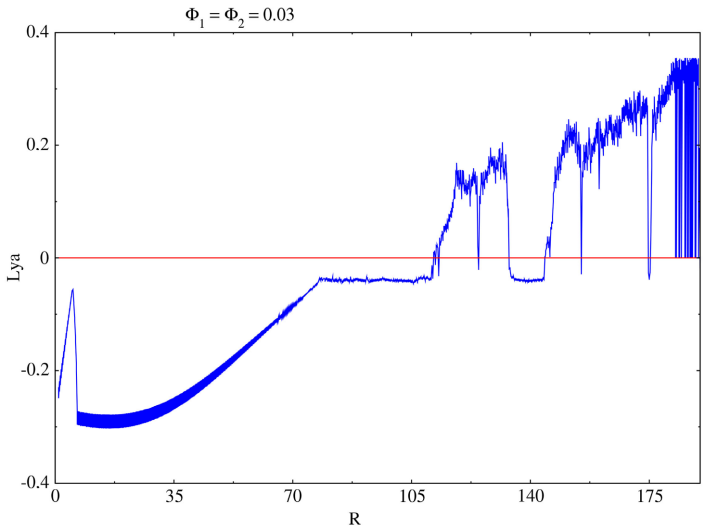

Figure 5. Bifurcation diagram and its corresponding Lyapunov exponent for (magnetite-copper)/water hybrid nanofluid ($\phi_1 = 0.03$, $\phi_2 = 0.03$) with the parameter values in **Table 1** and **Table 2**.

Figure 6 and **Figure 7** show the Bifurcation diagram and the corresponding Lyapunov exponent for the mono-nanofluids ($\phi_1 = 0, \phi_2 = 0.02$) and ($\phi_1 = 0.02$, $\phi_2 = 0$) respectively for (Copper-Water) and (Magnetite-Water) for the other parameter values in **Table 1** and **Table 2**. The observed dynamics are similar to those of the hybrid nanoliquid $\phi_1 = \phi_2 = 0.01$ in **Figure 3**. This observation could be justified by the fact that the total volume fraction ϕ is the same for the mono-nanofluid and the hybrid nanofluid ($\phi = \phi_1 + \phi_2 = 0.02$).

These different dynamics, observed through the bifurcation diagrams in **Figures 2-5**, were confirmed by their Lyapunov exponents and reconfirmed by the phase spaces and time evolutions for specific parameter values chosen within targeted intervals of the control parameter R in **Figure 2**, **Figure 3** and **Figure 5**. Thus, the volume fractions have a stabilizing effect on the hybrid nanofluids of (magnetite-copper)/water.

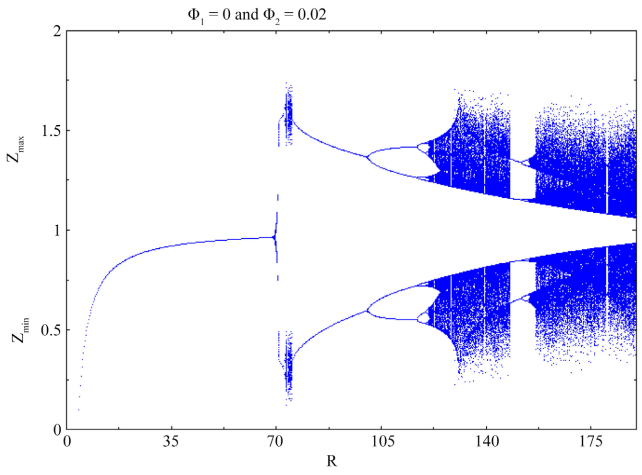

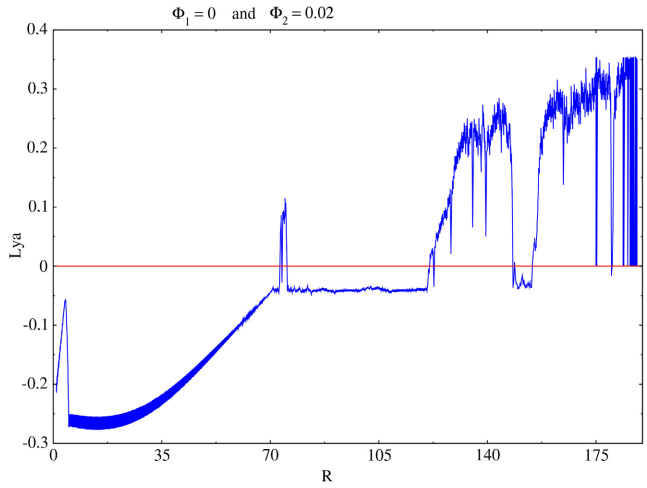

Figure 6. Bifurcation diagram and its corresponding Lyapunov exponent for copper-nanofluid ($\phi_1 = 0$, $\phi_2 = 0.02$), with the parameter values in Table 1 and Table 2.

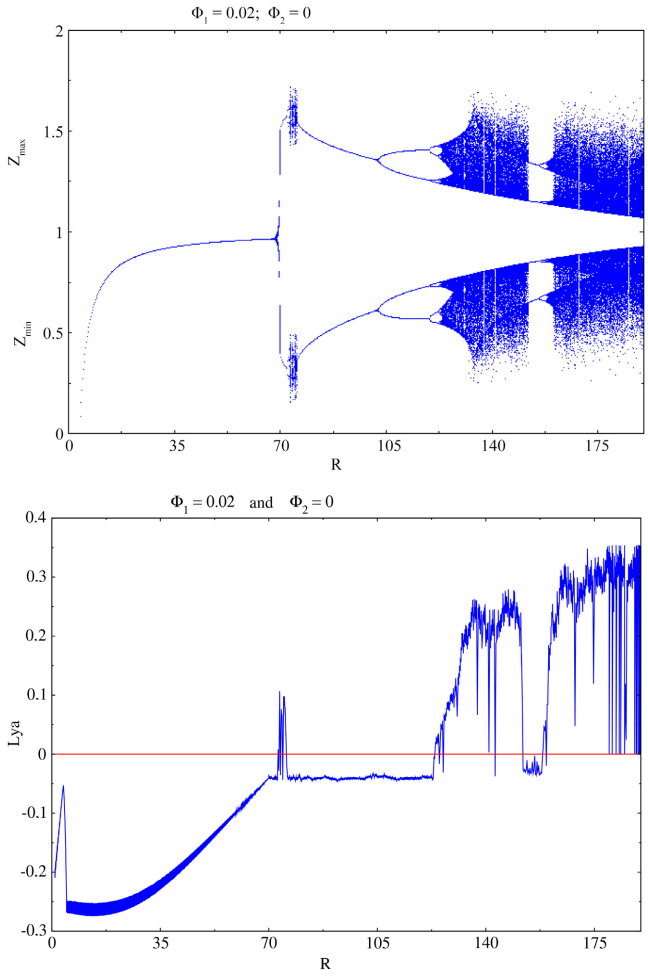

Figure 7. Bifurcation diagram and its corresponding Lyapunov exponent for magnetite nanofluid ($\phi_1 = 0.02$, $\phi_2 = 0$), with the parameter values in Table 1 and Table 2.

Figure 8 presents phase portrait in plane (Z, X) and its corresponding time

histories $z(t)$ respectively for ($\phi_1 = \phi_2 = 0$), ($\phi_1 = \phi_2 = 0.01$) and ($\phi_1 = \phi_2 = 0.03$); $R = 77$ and parameter values of Figure 2, Figure 3 and Figure 5. She shows, for $R \in]65,80[$, the interval in which the behavior gradually changes from chaotic to regular when going from the base fluid $\phi_1 = 0$, $\phi_2 = 0$ (water) to the hybrid nanofluids $\phi_1 = \phi_2 \neq 0$, the phase portraits and the time histories indeed showed a transition from chaos (pure water) to an oscillation $\phi_1 = 0.02$, $\phi_2 = 0.03$ passing through a periodic motion with period 2.

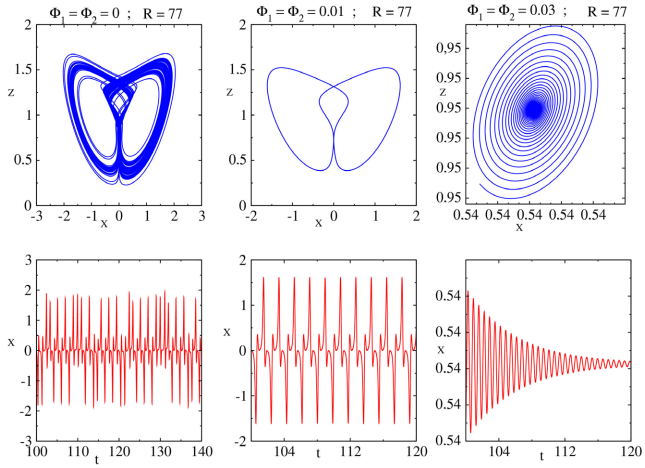

Figure 8. Phase space in plane (Z, X) and its corresponding time histories ($\phi_1 = 0 = \phi_2 = 0$), ($\phi_1 = \phi_2 = 0.01$) ($\phi_1 = \phi_2 = 0.03$), $R = 77$ and parameters values of Figure 2, Figure 5 and Figure 7.

Figure 9 presents phase portrait in plane (Q, X) and the corresponding time histories (Q, t) for water ($\phi_1 = \phi_2 = 0$) for the parameter values in Figure 9 for three different values of the control parameter $R = 90,124,141$. This figure shows the transitions from periodic, with periods of 1 and 2 to chaotic.

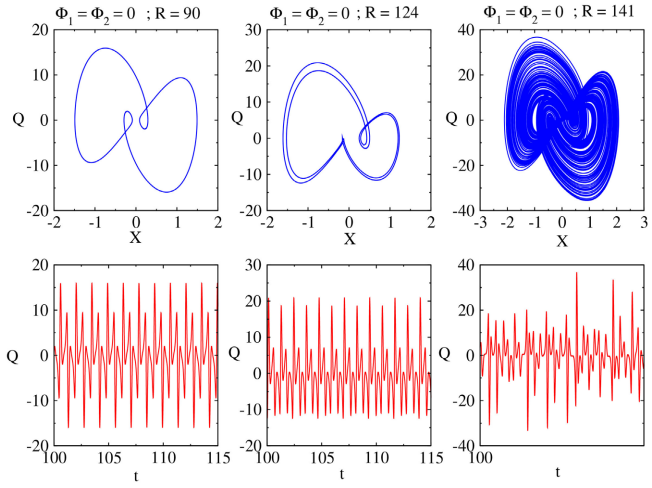

Figure 9. Phase space in plane (Q, X) and its corresponding time histories for ($\phi_1 = \phi_2 = 0$) and parameters values of Figure 2 respectively for $R = 90$, $R = 124$ and $R = 141$, with the parameter values in Table 2 and in Figure 3.

Figure 10 is plotted for two different values of the Solutal Rayleigh number $R_S = 20,30$, we note a reduction in the chaoticity domain of the hybrid nanofluid when the value R_S increases. We deduce that the Solutal Rayleigh number also has a stabilizing effect.

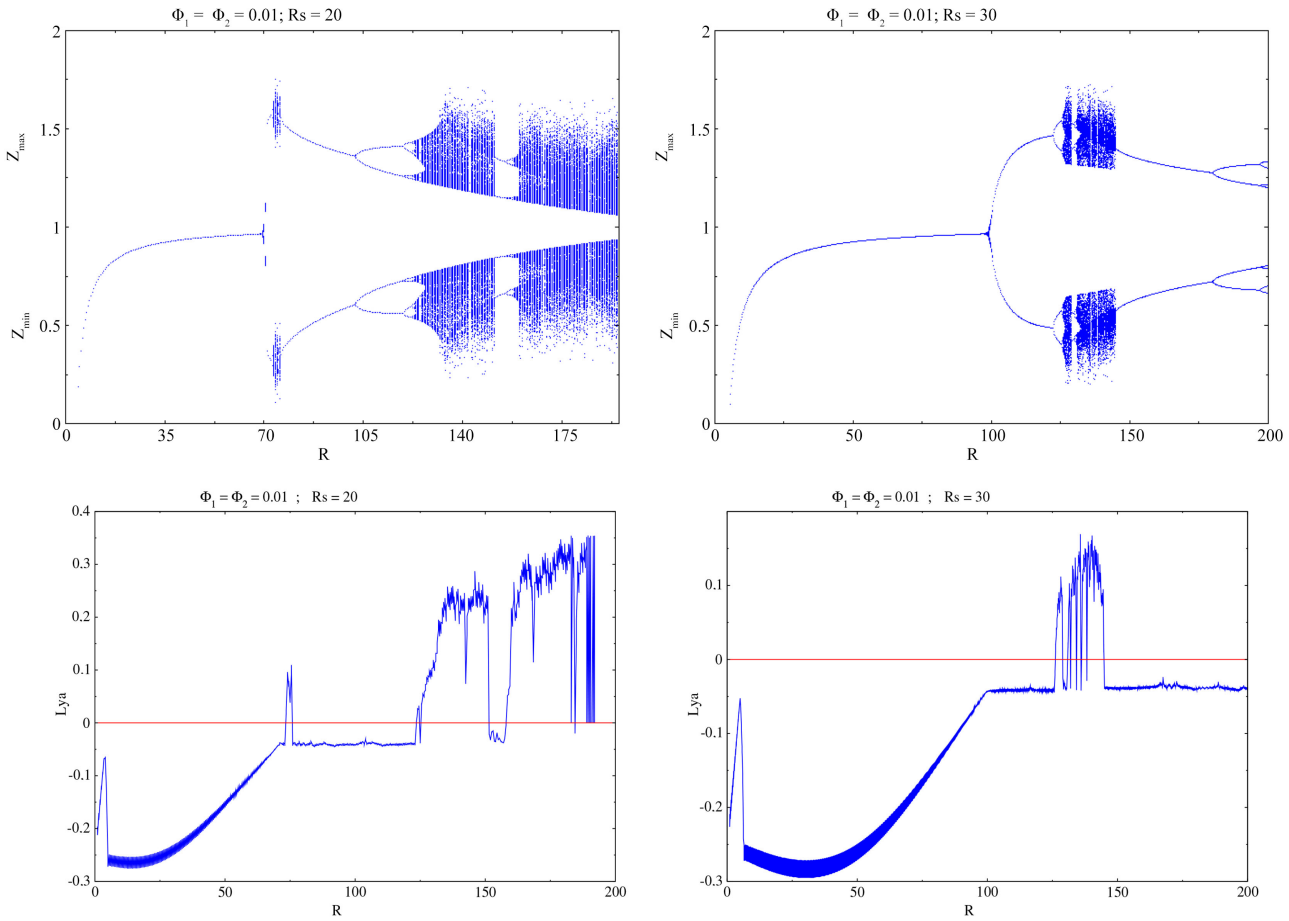

Figure 10. Bifurcation diagram and its corresponding Lyapunov exponent for (magnetite-copper)/water hybrid nanofluid ($\phi_1 = \phi_2 = 0.01$) respectively for $R_S = 20$ and $R_S = 30$, with the parameter values in Table 1 and Table 2.

Figure 11 shows the effect of Taylor number T_a on the bifurcation diagram and its corresponding Lyapunov exponent for hybrid nanoliquid ($\phi_1 = \phi_2 = 0.01$) of Figure 3, for the parameter values in Table 1 and Table 2, respectively for $T_a = 0.3$ and $T_a = 0.5$. We observe a rightward shift of the chaotic domain as the Taylor number increases. The Taylor number stabilizes hybrid nanoliquid regular convection by delaying the onset of chaotic convection.

To confirm the dynamics observed in the bifurcation diagrams of Figure 11, we constructed in Figure 12 the phase portraits for $R = 102$ and $R = 125$ for $T_a = 0.3$ and $T_a = 0.5$. At $R = 102$, the phase portraits show chaotic dynamics for $T_a = 0.3$ and regular dynamics for $T_a = 0.5$. On the other hand, at $R = 125$, the phase portraits show regular dynamics for $T_a = 0.3$ and chaotic dynamics for $T_a = 0.5$.

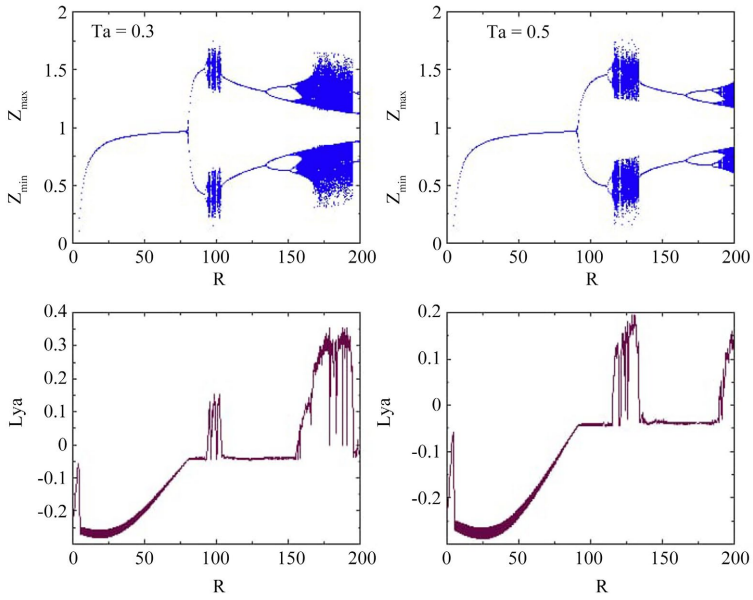

Figure 11. Bifurcation diagram and its corresponding Lyapunov exponent for water ($\phi_1 = \phi_2 = 0.01$); effects of Taylor number: $T_a = 0.3$ and $T_a = 0.5$ with the parameter values in Table 2 and Figure 3.

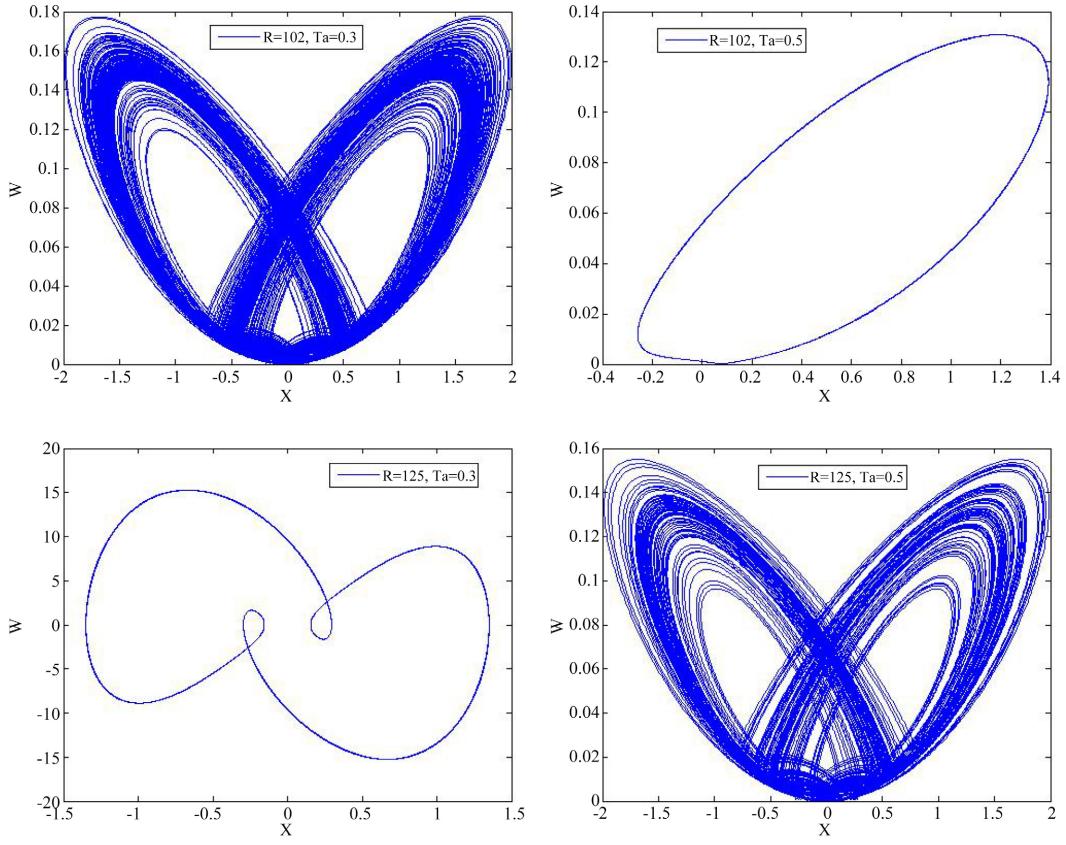

Figure 12. Phase space in plane (W, X) with ($\phi_1 = \phi_2 = 0.01$), $R_s = 20$; effects of Taylor number: top left ($T_a = 0.3$, $R = 102$); top right ($T_a = 0.5$, $R = 102$); bottom left ($T_a = 0.3$, $R = 125$); and bottom right ($T_a = 0.5$, $R = 125$) with the parameter values in Table 2 and in Figure 11.

Figure 13 shows effect of Darcy number D_a on the bifurcation diagram and its corresponding Lyapunov exponent for hybrid nanoliquid ($\phi_1 = \phi_2 = 0.01$) of Figure 3 for the parameter values in Table 1 respectively for $D_a = 0.005$ and $D_a = 0.05$.

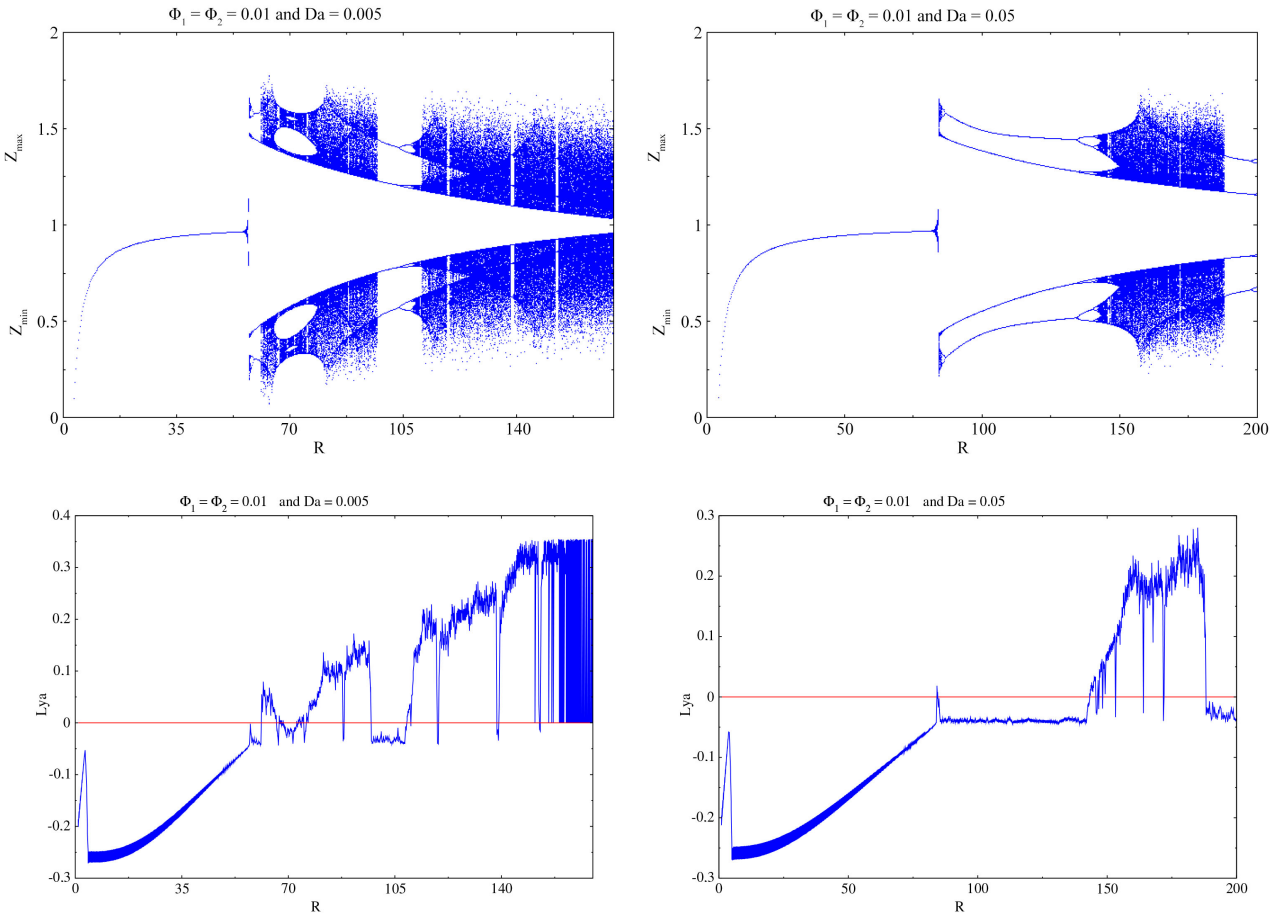

Figure 13. Bifurcation diagram and its corresponding Lyapunov exponent for hybrid nanoliquid ($\phi_1 = \phi_2 = 0.01$); effects of Darcy number: $D_a = 0.005$ and $D_a = 0.05$ with the parameter values in Table 2 and in Figure 6.

5. Conclusion and Suggestions

The chaotic convection of a hybrid (magnetite-copper)/water nanoliquid saturating a rotating porous channel was investigated. We used the Darcy-Bénard model with the Boussinesq approximation to model the thermosolutal convection of the hybrid nanofluid using partial differential equations. These equations were transformed using the minimum order double Fourier series method, based on the truncated Galerkin approximation. After this transformation, we obtained a modified Lorenz system of order six. We obtained a negative value for the trace of the Jacobian matrix associated with this system, which characterizes its dissipative nature. We were able to identify three fixed points for the system: one trivial, which is the origin, and two non-trivial ones. We performed numerical simulations using Fortran and a fourth-order Rung-Kutta algorithm to plot bifurcation diagrams,

Lyapunov exponents, phase portraits, and amplitude evolutions over time. Analysis of the bifurcation diagrams shows that the system can transition from regular (periodic or quasi-periodic) to chaotic behavior, and vice versa, depending on the parameter values. These dynamics observed in the bifurcation diagrams were confirmed by the Lyapunov exponents, as well as by the phase portraits and amplitude evolutions over time. We observed that increasing the volume fraction stabilizes the convection of the hybrid nanofluid by reducing or even eliminating the initial chaotic domain. We also found that increasing the Solutal Rayleigh number has a stabilizing effect on the convection of the water hybride nanofluid. The Taylor number, on the other hand, stabilizes the convection of this nanofluid by delaying its chaotic behavior. Increasing the Darcy parameter, on the other hand, considerably reduces the chaotic convection domain in favor of regular behavior. We can conclude that concentration, porosity, and nanoparticles (Fe_3O_4-Cu) can serve as parameters to control the convection of the hybrid nanoliquid (Fe_3O_4-Cu)/water. The results obtained will serve as a basis in process engineering for the synthesis of new heat transfer fluids to regulate energy transfer in industrial facilities. A thorough study of this modified Lorenz system, focusing on the stability of its fixed points, will allow us to investigate its Hopf bifurcation.

Acknowledgements

The authors wish to thank the "Institut National Supérieur de Technologie Industrielle" (INSTI)/UNSTIM for its support through the PFC-R Edition 2, as well as Doctors M. L. Hounvenou and S. J. Dèdèwanou for their technical contributions.

Conflicts of Interest

The authors declare no conflicts of interest regarding the publication of this paper.

References

[1] Zada, L., Ullah, I., Alqahtani, A. M., Nawaz, R., Khan H. and Alam, K., Khan H. and A Zada, L., Ullah, I., Alqahtani, A.M., Nawaz, R., Khan, H. and Alam, K. (2024) Enhancing Energy Efficiency and Heat Transfer Performance of Engine Oil Flow through Hybrid Nanoparticles in Convergent/Divergent Channel. *Results in Engineering*, **22**, Article ID: 102027. https://doi.org/10.1016/j.rineng.2024.102027

[2] Ahmad, S., Ali, K., Nisar, K.S., Faridi, A.A., Khan, N., Jamshed, W., *et al.* (2021) Features of Cu and TiO_2 in the Flow of Engine Oil Subject to Thermal Jump Conditions. *Scientific Reports*, **11**, Article No. 19592. https://doi.org/10.1038/s41598-021-99045-x

[3] Dèdèwanou, S.J., Diallo, T.M.P., Doumbouya, M.B., Sylla, M.C., Camara, F. and Hinvi, A.L. (2025) Combined Effects of Magnetic Field and Nanoparticles on Rotating Engine-Oil Flow Using a New Local Thermal Non-Equilibrium Formulation. *Open Journal of Fluid Dynamics*, **15**, 64-86. https://doi.org/10.4236/ojfd.2025.152005

[4] Choi, S.U.S. and Eastman, J.A. (1995) Enhancing Thermal Conductivity of Fluids with Nanoparticles. *Proceedings of the ASME International Mechanical Engineering Congress and Exposition*, San Francisco, 12-17 November 1995, 99-106.

[5] Das, S.K., Choi, S.U.S., Yu, W. and Pradeep, T. (2007). Nanofluids: Science and Tech-

nology. John Wiley & Sons, 64-86.

[6] Buongiorno, J. (2005) Convective Transport in Nanofluids. *Journal of Heat Transfer*, **128**, 240-250. https://doi.org/10.1115/1.2150834

[7] Khanafer, K., Vafai, K. and Lightstone, M. (2003) Buoyancy-Driven Heat Transfer Enhancement in a Two-Dimensional Enclosure Utilizing Nanofluids. *International Journal of Heat and Mass Transfer*, **46**, 3639-3653. https://doi.org/10.1016/s0017-9310(03)00156-x

[8] Oztop, H.F. and Abu-Nada, E. (2008) Numerical Study of Natural Convection in Partially Heated Rectangular Enclosures Filled with Nanofluids. *International Journal of Heat and Fluid Flow*, **29**, 1326-1336. https://doi.org/10.1016/j.ijheatfluidflow.2008.04.009

[9] Sheikholeslami, M., Gorji-Bandpy, M., Ganji, D.D. and Soleimani, S. (2014) Thermal Management for Free Convection of Nanofluid Using Two Phase Model. J*ournal of Molecular Liquids*, **194**, 179-187. https://doi.org/10.1016/j.molliq.2014.01.022

[10] Abedini, A., Armaghani, T. and Chamkha, A.J. (2018) MHD Free Convection Heat Transfer of a Water-Fe_3O_4 Nanofluid in a Baffled C-Shaped Enclosure. *Journal of Thermal Analysis and Calorimetry*, **135**, 685-695. https://doi.org/10.1007/s10973-018-7225-8

[11] Devi, S.S.U. and Devi, S.P.A. (2017) Heat Transfer Enhancement of Cu-Al_2O_3/Water Hybrid Nanofluid Flow over a Stretching Sheet. *Journal of the Nigerian Mathematical Society*, **36**, 419-433.

[12] Sajjadi, H., Amiri Delouei, A., Sheikholeslami, M., Atashafrooz, M. and Succi, S. (2019) Simulation of Three Dimensional MHD Natural Convection Using Double MRT Lattice Boltzmann Method. *Physica A*: *Statistical Mechanics and its Applications*, **515**, 474-496. https://doi.org/10.1016/j.physa.2018.09.164

[13] Lorenz, E.N. (1963) Deterministic Nonperiodic Flow. *Journal of the Atmospheric Sciences*, **20**, 130-141. https://doi.org/10.1175/1520-0469(1963)020<0130:dnf>2.0.co;2

[14] Sparrow, C. (1982) The Lorenz Equations: Bifurcations, Chaos, and Strange Attractors. Springer.

[15] Ruelle, D. and Takens, F. (1971) On the Nature of Turbulence. *Communications in Mathematical Physics*, **20**, 167-192. https://doi.org/10.1007/bf01646553

[16] Guckenheimer, J. and Holmes, P. (1983) Nonlinear Oscillations, Dynamical Systems, and Bifurcations of Vector Fields. Springer, 20 p.

[17] Cattaneo, C. (1958) A Form of Heat Conduction Equation Which Eliminates the Paradox of Instantaneous Propagation. *Comptes Rendus de l'Académie des Sciences*, **247**, 431-433.

[18] Joseph, D.D. and Preziosi, L. (1989) Heat Waves. *Reviews of Modern Physics*, **61**, 41-73. https://doi.org/10.1103/revmodphys.61.41

[19] Siddheshwar, P.G., Kanchana, C. and Laroze, D. (2021) A Study of Darcy-Bénard Regular and Chaotic Convection Using a New Local Thermal Non-Equilibrium Formulation. *Physics of Fluids*, **33**, Article ID: 044107. https://doi.org/10.1063/5.0046358

[20] Makinde, O., Khan, W. and Khan, Z. (2017) Stagnation Point Flow of MHD Chemically Reacting Nanofluid over a Stretching Convective Surface with Slip and Radiative Heat. *Proceedings of the Institution of Mechanical Engineers*, *Part E*: *Journal of Process Mechanical Engineering*, **231**, 695-703. https://doi.org/10.1177/0954408916629506

[21] Bachok, N., Ishak, A., Nazar, R. and Pop, I. (2020) Flow and Heat Transfer at a General 3-D Stagnation Point in a Nanofluid. *Physica B*: *Condensed Matter*, **405**, 4914-

4918. https://doi.org/10.1016/j.physb.2010.09.031

[22] Idris, R., Siri, Z. and Hashim, I. (2013) On a Five-Dimensional Chaotic System Arising from Double-Diffusive Convection in a Fluid Layer. *Abstract and Applied Analysis*, **2013**, Article ID: 428327. https://doi.org/10.1155/2013/428327

[23] Rahmatinejad, B., Abbasgholipour, M. and Alasti, B. M. (2021) Investigating Thermophysical Properties and Thermal Performance of Al_2O_3 and CuO Nanoparticles in Water and Ethylene Glycol Based Fluids. *International Journal of Nano Dimension*, **12**, 252-271.

[24] Elsaid, E.M. and Abdel-wahed, M.S. (2022) MHD Mixed Convection Ferro Fe_3O_4/Cu-Hybrid-Nanofluid Runs in a Vertical Channel. *Chinese Journal of Physics*, **76**, 269-282. https://doi.org/10.1016/j.cjph.2021.12.016